REPORT DOCUMENTATION PAGE

AFRL-SR-BL-TR-98-

0158

ources,
of this
fferson

1. AGENCY USE ONLY (Leave blank)	2. REPORT DATE	3. REPORT TYPE AND DATES COVERED
		Final 01 Jul 95 to 30 Sep 97

4. TITLE AND SUBTITLE

All fiber-based optical transmitters and switching Technolgies

5. FUNDING NUMBERS

61101E
C486/01

6. AUTHOR(S)

Professor Cheo

7. PERFORMING ORGANIZATION NAME(S) AND ADDRESS(ES)

University of Connecticut
343 Mansfield Rd, U151
Storrs, CT 06269-2151

8. PERFORMING ORGANIZATION REPORT NUMBER

9. SPONSORING / MONITORING AGENCY NAME(S) AND ADDRESS(ES)

AFOSR/NE
110 DuncaN Ave RmB115
Bolling AFB DC 20332-8050

10. SPONSORING / MONITORING AGENCY REPORT NUMBER

F49620-95-1-0463

11. SUPPLEMENTARY NOTES

12a. DISTRIBUTION / AVAILABILITY STATEMENT

APPROVAL FOR PUBLIC RELEASE: DISTRIBUTIONS UNLIMITED

19980218 039

13. ABSTRACT *(Maximum 200 words)*

A coupled-cavity mode-locked fiber laser using three Bragg grating in tandem has been demonstrated. The matching of cavity lengths of the two cou;ed cavities is not critical and the difference in length can be as large as 2mm still achieving mode-looking. The pulse width of these mode-locked lasers is, longer than the transform-limited value Er-doped fiber lasers are very unstable an usually exhibit self-pulsing behavior. Using a high-gain Er-doped fiber, the instablity caused by resonant pump perturbation can be suppressed. One method to suppress the self-pulsing problem is to increase the emission to absorption ratio. Another methold is to introduce Ytterbium ions (Yb) into Er-doped fiber. Samples of non-linear CdSSe-doped fibers have been fabricated for single mode operation in the wavelength region between 980nm-1550nm. Linear absorption coefficenty was found to be 0.14 dB/cm at 1550 nm. The nonresonant nonlinear refractive index was found to be 1.8x10-17m2/W, 400 times greater than silica fiber.

14. SUBJECT TERMS			15. NUMBER OF PAGES
			16. PRICE CODE
17. SECURITY CLASSIFICATION OF REPORT	18. SECURITY CLASSIFICATION OF THIS PAGE	19. SECURITY CLASSIFICATION OF ABSTRACT	20. LIMITATION OF ABSTRACT
UNCLASSIFIED	UNCLASSIFIED	UNCLASSIFIED	UL

NSN 7540-01-280-5500

Standard Form 298 (Rev. 2-89)
Prescribed by ANSI Std. 239-18

ALL FIBER BASED OPTICAL TRANSMITTERS AND SWITCHING TECHNOLOGIES

FINAL TECHNICAL REPORT

Submitted by

P.K. Cheo and E. Donkor
University of Connecticut
Storrs, CT 06269

Project Sponsor: AFOSR/DARPA
Contract No. F49620-95-1-0463
Contract Period: July 1995 to December 1997

TABLE OF CONTENTS

1. PROJECT SUMMARY

A two-year research and development program focuses on technologies in fiber lasers and fiber switches utilizing intra-core Bragg gratings and CdS Se nonlinear fibers.

Under this program, a coupled-cavity mode-locked fiber laser using three Bragg grating in tandem has been demonstrated. Results indicate that the matching of cavity lengths of the two coupled cavities is not criitcal and the difference in length can be as larege as 2 mm still achieving mode-locking. This behavior is attributed to the time delay compensation effect by the Bragg gratings. However, the pulse width of these mode-locked lasers is, in general, much longer than the transform-limited value dictated by the bandwidth of the gratings.

A major effort was made to investigate the stability of fiber lasers. Our results as well as others show that Er-doped fiber lasers are very unstable and usually exhibit self-pulsing behavior. Both theoretical and experimental research was conducted. Results show that by using a high-gain Er-doped fiber, the instability caused by resonant pump perturbation can be suppressed. One method to suppress the self-pulsing problem is to incrase the emission to absorption ratio. Another method is to introduce Ytterbium ions (Yb) into Er-doped fiber. With a high codoping concentration ratio (~10 to 1) it is possible to suppress self-pulsing, which is basically caused by the so-called ion-pair formation in highly concentrated Er-doped fiber.

Also under the program, samples of non-linear CdSSe-doped fibers have been fabricated for single mode operation in the wavelength region between 980nm - 1550nm. The linear absorption coefficient of the fiber samples were measured, using the cut-back method, and found to be 0.14 dB/cm at 1550nm. The transmittivity of the fiber covering the wavelength range is between 800nm and 1600nm. Using the z-scan method, the nonresonant nonlinear refractive index n_2 of the fiber was also measured and found to be $1.8 \times 10^{-17} m^2/W$. This value of n_2 is about 400 times greater than silica fiber.

2. Objective

The objective of this program is to achieve a compact and low cost package of an integrated optical mode-locked fiber laser with an optically pumped fiber switch suitable for extremely broadband all optical networks. Toward this objective, a two-year research and development program was conducted and has been focused on the already developed technologies at UConn involving the fiber lasers using intra-core Bragg gratings and the CdSSe fiber switches having extremely high non-linear coefficients. The goal is not only to achieve ultra-short pulses from in-line coupled cavity fiber lasers and very short fiber switches, but also to demonstrate their usefulness and suitability for high bit rate optical fiber communication networks. Research and development of low-cost, simple and reliable transmitter suitable for time-division multiplexing (TDM) and/or wavelength-division multiplexing (WDM) is essential for future light-wave communication systems.

3. Mode-Locked Fiber Lasers

Passive mode-locking of fiber lasers in the figure eight [1] and in the ring configuration [2] have been reported. Coupled-cavity mode-locking of fiber lasers using bulk optics has also been reported [3]. In this report we have generated very stable mode-locked laser pulses from an in-line coupled-cavity fiber laser using three intra-core Bragg gratings. The theory of passive mode-locking is well understood. Using the non-linear model of a coupled-cavity with a non-linear index, we constructed three in-line coupled cavity fiber lasers, A, B and C, all of which employ Er-doped fiber as main laser cavity, and a non-linear silica fiber of the same length as the auxiliary cavity. Two intra-core Bragg gratings are used to form the main cavity and a third intra-core Bragg grating is used to form the coupled cavity. Fig. 1 depicts the experimental setup.

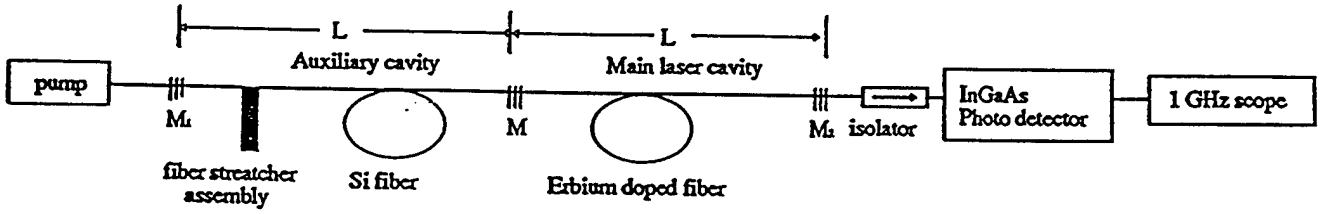

Fig. 1 Schematic diagram of the in-line fiber laser experimental set-up.

Table I summarizes the Bragg grating's parameters used for these lasers. All lasers were constructed with a cavity length of 47cm/47cm by using a high-gain

Er-doped fiber (30dB/m). The parameters of lasers A and B are the same except that the central coupling gratings have different reflectivity and spectral bandwidth as shown in Table I.

TABLE I
SPECTRAL CHARACTERISTICS OF BRAGG GRATINGS USED IN THE NEW 47 cm COUPLED-CAVITY FIBER LASERS

	47cm/47cm laser A			47cm/47cm laser B			47cm/47cm laser C		
	a	b	c	a	b	c	a	b	c
Reflectivity (%)	91	95	99.5	91	80	99.5	80	91	99.5
Spectral peak (nm)	1530.3	1530.5	1530.4	1530.3	1530.4	1530.4	1530.4	1530.3	1530.4
Spectral width (nm)	0.5	0.2	0.5	0.5	0.5	0.5	0.5	0.5	0.5

Self-start mode-locking is always observable from laser A and B without any cavity length control for optical phase matching. Fig. 2 shows an oscilloscope trace of the output pulse train of laser B at a pump level of 50mW, where the time resolution is limited by the 1 GHz bandwidth of the photodiode (PD) detector. The frequency response characteristics of the detecting circuit causes the baseline to drift slightly in Fig. 2. The measured average output power from lasers A and B as a function of the input pump power is plotted in Fig. 3, which shows that laser A has a lower slope-efficiency than laser B. The output power and pulses coming from laser B are very stable, but the output power of laser A varies alternately between two levels event though stale pulses can be observed. This bi-stable behavior is most likely caused by the mismatch of the grating spectral bandwidth in laser A.

To improve the output power, we modified laser B simply by exchanging the two grating of the main cavity to construct a laser C. In doing so, the output coupling is doubled for laser C while keeping the laser cavity Q-value the same. But the coupling between the two cavities becomes weak. The average output power of laser C is increased by nearly 60% from that of laser B as shown in Fig. 3, and the lasing threshold has an extrapolated value of approximately 1mW. There are two distinct slope efficiencies αCW and αML for each laser, which associate with the onset of CW oscillation near the threshold and the mode-locked operation, respectively. As the CW output power reaching a level of ~0.2 mW, self-mode-locking begins with a pulse output increasing linearly with pump power. We write

$$P_{ML} = 0.2mW + \alpha_{ML} P_{pump}$$

where α_{ML} = 0.1%, 0.7% and 1.4% for lasers A, B and C, respectively. It appears that there exists a residual CW laser radiation in all mode-locked fiber lasers studied as can be seen from Fig. 2. The CW background is expected to be decreased by increasing the coupling strength between the cavities. The pulse repetition rate for lasers A, B and C is 213 MHz, which is in accordance with the round trip time of optical pulses in the cavities.

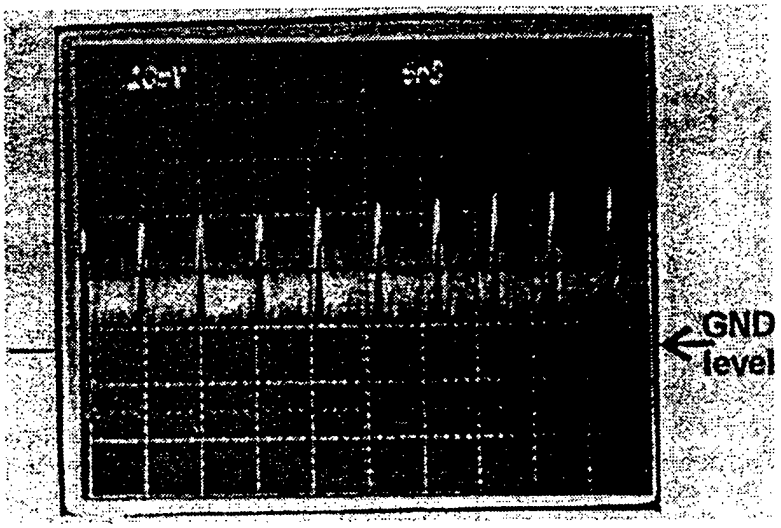

Fig. 2. Oscilloscope trace of output pulse train of laser B at 50 mW pump level observed with a PD (1 GHz bandwidth).

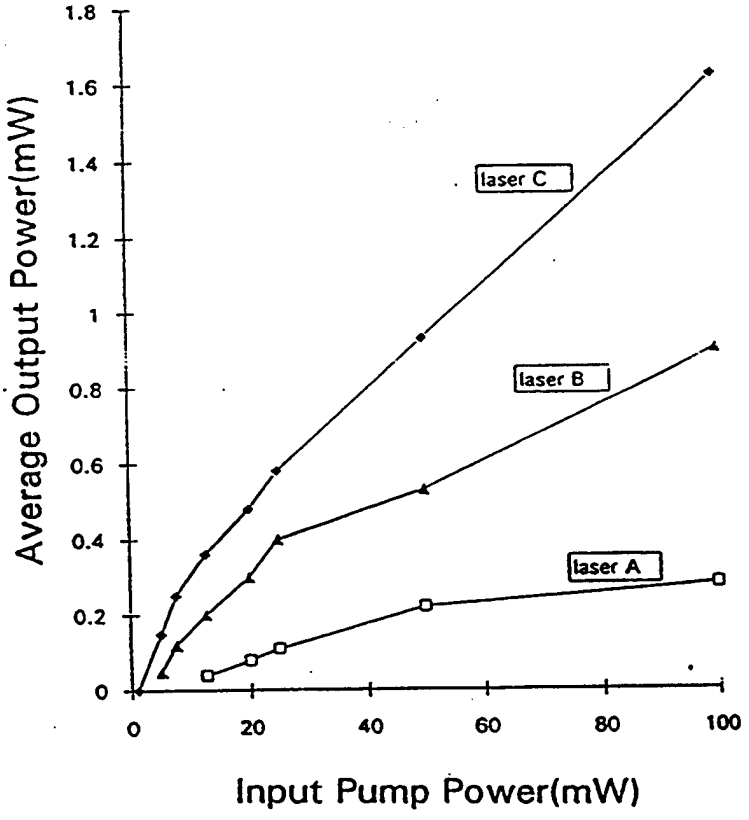

Fig. 3. Average output power at 1530 nm versus input pump power at 980 nm for lasers A, B, and C.

To measure the pulse widths generated by the mode-locked fiber lasers, a background-free autocorrelator (INRAD 5-14 B) was used. The autocorrelation trace and spectrum of output pulses from laser B at a pump level of ~100 mW is shown in Fig. 4. The pulse width is ~60 ps with an assumption of Gaussian pulse and the spectrum, which is a superposition of the mode-locked pulses and CW light, has a 3-dB bandwidth of 0.5 nm. The spectral components with a sharp edge at the longer wavelength side is considered coming from the CW oscillation. The output pulse widths of laser A and laser C are longer than that of laser B and the autocorrelations are a little larger than the 119 ps dynamic range of our autocorrelator. Also, the pulse width of laser B increases with the pump level, and is measured to be larger than the 84 ps equipment limit at a pump power of 250 mW. The output of all the lasers was monitored by the PD and the oscilloscope during the experiment. Pulse trains similar to that shown in Fig. 2 can always be observed in mode-locked operation. This means that the measured background-free autocorrelation is indeed mode-locked pulse but not coherent noise spikes. Because of the 1 GHz-bandwidth limit of the PD detector, the peak power of the mode-locked pulses is difficult to get with the oscilloscope, and is estimated to be in an order of about 0.1 W.

Under the condition that three gratings are matched and the length difference ΔL between the main and auxiliary cavities is adjusted to be small enough, the coupled-cavity fiber lasers investigated in our experiments always provide mode-locked pulses without the need of a precise cavity length controlling which is usually necessary for APM mode-locked lasers [4]. Attempts were made to tune the optical phase in the auxiliary cavity by heating a section of the fiber, but we did not observe any noticeable effect on the mode-locked pulse train.

The optical phase matching relation required a stable interaction between the coupled cavities may be self-adjustable by means of the laser oscillating wavelength λ when the cavity length difference ΔL is much larger than λ. That is, a constructive feedback wave from the auxiliary cavity makes the total loss of the main cavity smallest and the wavelength satisfying this phase condition becomes the oscillating wavelength λ when $\Delta L >> \lambda$. To get the additive pulse mode-locking effect and suppress the CW oscillation, a destructive initial phase-setting is required for APM lasers [5], therefore ΔL must be adjusted to have the same order as λ so that the optical phase can be controlled by adjusting ΔL.

However, the conditions of $\Delta L \sim \lambda$ can be relaxed for the mode-locking of a coupled-cavity laser. This is evident from the experimental result on a mode-locked coupled-cavity laser with a saturable absorber in the auxiliary cavity [6]. There, mode-locking was achieved for ΔL =2mm ($>> \Delta L \lambda$). Our coupled-cavity fiber lasers using Bragg gratings with finite bandwidth also provide mode-locking with an estimated ΔL of 1~2 mm. The mechanism of the mode-locking behavior of our in-line coupled cavity fiber laser may be caused by the wavelength-dependent delay property of Bragg gratings [7]. It was shown that the non-linear

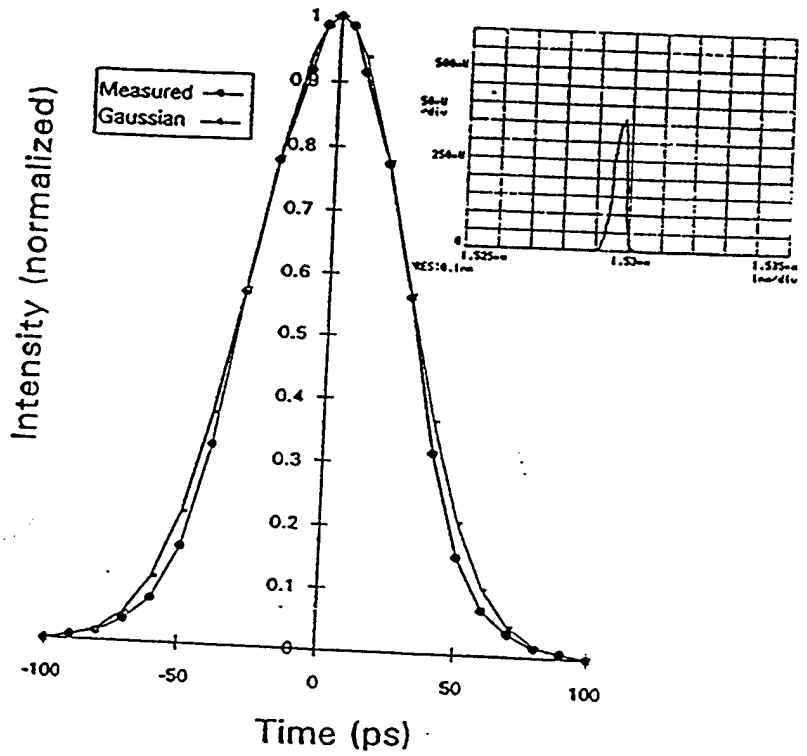

Fig. 4. Background-free auto correlation of the 60 ps pulses from laserB at 100 mW pump level, and the output spectrum (inset).

dependence of phase of the reflection coefficient on wavelength causes a different delay time when reflected by a Bragg grating.

4. The Stability Study

4.1 Relaxation Oscillation

We first present our analysis on the power fluctuation in fiber lasers caused by resonant diode pump power perturbation. We show that this fluctuation is inversely proportional to photon life time (Ref. 8.). We also show that such instability caused by resonant pumping perturbation can be suppressed by using high-gain fibers. By solving the rate equations (Ref. 8.) involving the upper laser level population density and photon density q_0, we obtain a simple (approximate) expression for photon fluctuation function q_m as given by

$$\frac{q_m}{q_0} = \frac{1}{\omega_m \tau_c} \frac{R_m}{R_{p0}} \qquad (1)$$

where the oscillation frequency ω_m is given by

$$\omega_m = \sqrt{R_{p0} N_0 r_q} \qquad (2)$$

R_0 and R_m are unperturbed and perturbed pump rates, respectively. $r_q = c\sigma_2/n$ where σ_2 is the absorption cross section. τ_c is the photon cavity lifetime. N_0 is Er doping concentration which is about $3\times10^{19}/cm^3$. Figure 5 shows the variation of relative fluctuation of photon density as a function of τ_c. The solid curve is the result obtained from the approximate expression (1). The square points are the results obtained by solving the rate equations numerically. We see that the approximation is valid for $\tau_c \geq 4$ nsec. As an example, for $R_m/R_0 = 0.5\%$ and $\tau_c = 4$ nsec, a 30% photon density fluctuation is expected. Equations (1) and (2) indicate that the photon density fluctuation can be significantly suppressed by using a Er-doped fiber with a high-gain coefficient or high Er-doping concentration N_0. However, the use of high gain Er-doping fibers leads to a different set of problems. In particular, the self-pulsing instability due to ion-pair interactions becomes the dominant problem.

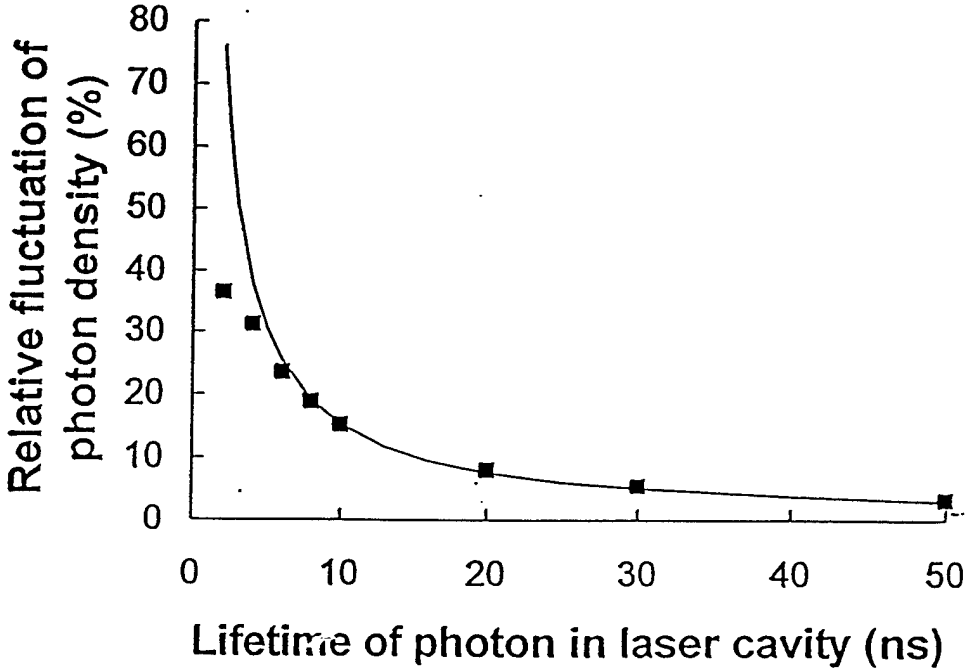

Fig. 5 Photon density fluctuation vs. photon lifetime.

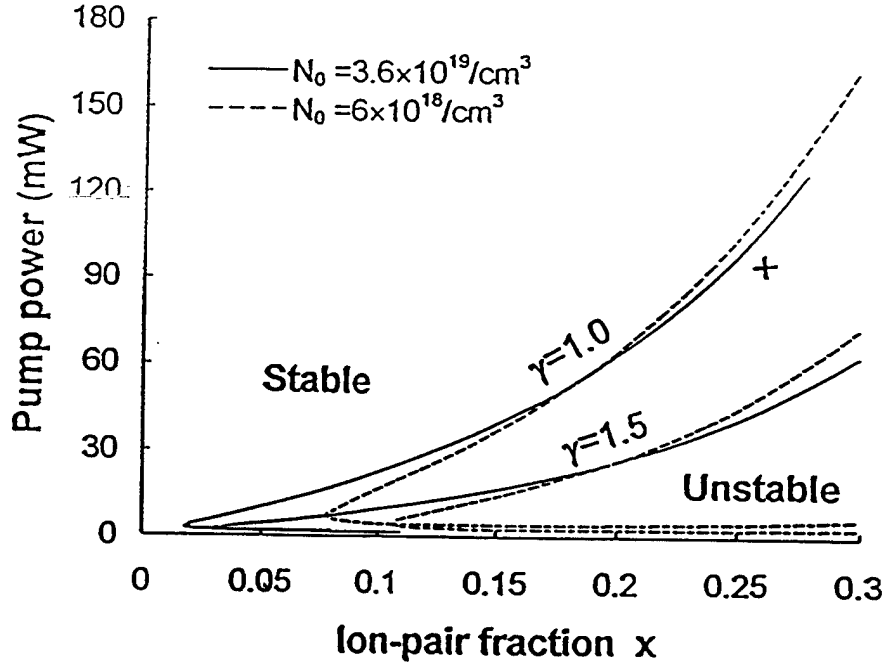

Fig. 6 Stability diagrams for various σ_a nd γ values but at a fixed τ_c= 10 n sec as a function of ion-pair fraction.

4.2 Ion-Pair Induced Self-Pulsing

We found that the ion-pair induced self-pulsing in Er-doped fiber lasers depends largely on the ratio γ of emission to absorption cross sections. Because of this dependence, self-pulsing can be suppressed by increasing the γ value. To treat this problem analytically, we solve the rate equations by using the model introduced by Sanchez and co-workers (Ref. 9). In this model, Er-ions are separated into two groups: isolated ions and ion-pairs. Isolated ions can be described by a two-level system, whereas the ion-pairs are described by a three-level system, which is comprised of the ground state n_1, one-ion excited state n_2, and an ion-pair excited state n_{ij}, (both ions excited). Coupled with the population of these three levels is the photon density, q. The laser dynamics are described by four coupled rate equations as given by (Ref. 8)

$$\frac{dn_2}{dt} = R_p(1-n_2) - qr_q[(\gamma+1)n_2 - 1] - \frac{n_2}{\tau_2} \tag{3}$$

$$\frac{dn_{11}}{dt} = -R_p n_{11} + q\alpha r_q[\gamma - (\gamma+1)n_{11} - \gamma n_{22}] + \frac{1-n_{11}-n_{22}}{\tau_2} \tag{4}$$

$$\frac{dn_{22}}{dt} = R_p(1-n_{11}-n_{22}) - q\alpha r_q[n_{11} + (\gamma+1)n_{22} - 1] - \frac{n_{22}}{\tau_{22}} \tag{5}$$

$$\frac{dq}{dt} = qr_q N_0\{(1-2x)[(\gamma+1)n_2 - 1] + \alpha x(\gamma - 1 - \gamma n_{11} + n_{22})\} - \frac{q}{\tau_c} \tag{6}$$

where

$$R_p = \frac{P_p}{h\nu_p A_{eff}}\sigma_p, \qquad r_q = \frac{c}{n}\sigma_a. \tag{7}$$

From (3) to (6) we obtain a set of steady-state solutions. The stability conditions can be determined by solving the eigen-values of the matrix [A] formed by a set of homogenous equations derived from (3) to (6).

For laser parameters above threshold, matrix [A] always has two real negative eigen-values and a pair of complex conjugate eigen-values, whose real part determines the stability of the laser. But when the real part is positive, any perturbation will increase with time exponentially and lead to unstable operation involving self-pulsing.

Fig. 6 and 7 give the calculated stability diagrams on the x-Pp plane. Fig 6 shows the dependence of laser stability on ion concentration N_0 and γ with a fixed photon life time τ_c =10 n sec. Fig. 7 shows the dependence of photon life time and γ with a fixed $N_0 = 8x10^{18}$ cm^{-3}. In all cases, when γ is increased from 1 to 1.5, the unstable area i.e. the pump power required to suppress self-pulsing is decreased by half or more for a given N_0 and τ_c. The calculated results are in good agreement with our experimental observations from two fiber lasers, one operating at λ = 1.531 um (γ = 1) and the other operating at λ = 1.56 um (γ=1.5). Er-doped fiber in these cases has a N_0 value equal to 3.6 x 10^{19} cm^{-3} corresponding to a gain coefficient of 55 dB/m. at 1.53 um.

4.3 Effects of Yb:Er Co-Doping

In Section 4.2 we show that ion-pair induced self-pulsing can be suppressed by increasing the emission to absorption cross section ratio of Er-ions. This approach has very limited usefulness because γ values cannot be increased freely. Another approach is to increase the pump rate to bleach the ion-pair effect. However, this is limited by the available diode laser pump power. To increase the pump efficiency, it has been demonstrated (Ref. 10) that the use of Yb:Er co-doped fiber can be very effective.

We have analyzed the Yb:Er system and derived a functional dependence of the effective pumping rate of Yb:Er co-doped fibers on fractional Er ion concentrations. We show that the Yb:Er co-doped fiber is very effective to suppress the ion-pair induced self-pulsing in Er doped fiber lasers. To investigate the effects of Yb on Er ions, we assume that Yb ion concentration is high enough to satisfy the fast diffusion limit, so that rate equations can be used to describe the energy transferring process. Using the same model (Ref. 11), we introduce one additional coupled rate equation for the Yb excited state population density as given by

$$\frac{dM_2}{dt} = R_p^{Yb}(M_0 - 2M_2) - \rho M_2 N_0[(1-2x)(1-n_2) + x(1-n_{22})] - \frac{M_2}{\tau_{Yb}} \quad (8)$$

Where M_1 and M_2 are the ground state and the excited state of Yb ion densities, respectively, and

$$R_p^{Yb} = \frac{P_p}{h\nu_p A_{eff}}\sigma^{Yb}, \qquad R_p^{Er} = \frac{P_p}{h\nu_p A_{eff}}\sigma_p, \qquad r_q = \frac{c}{n}\sigma_a. \quad (9)$$

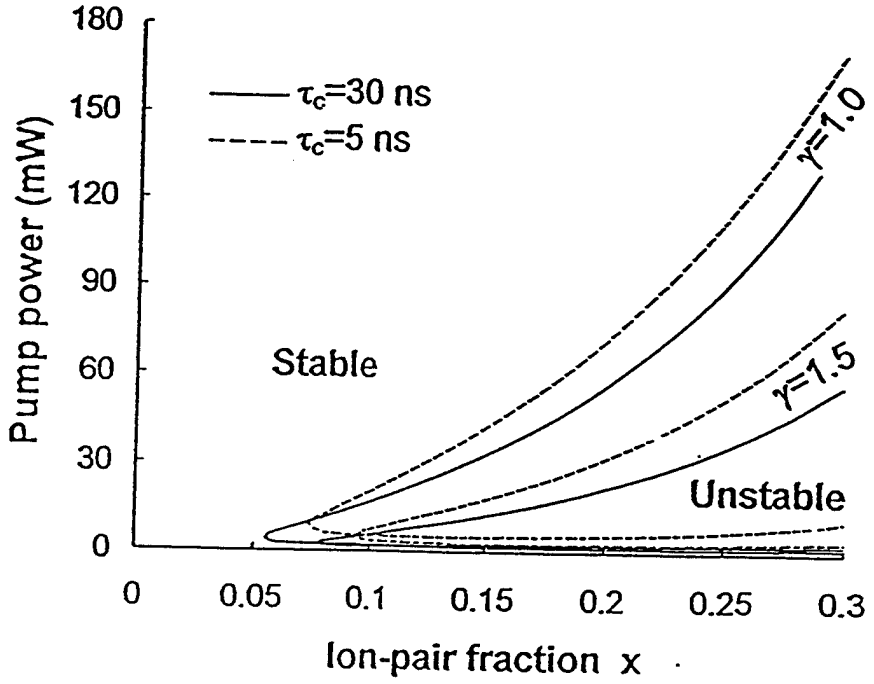

Fig. 7 Stability diagram for various σ_a, τ_c and γ values as a function of ion-pair fraction.

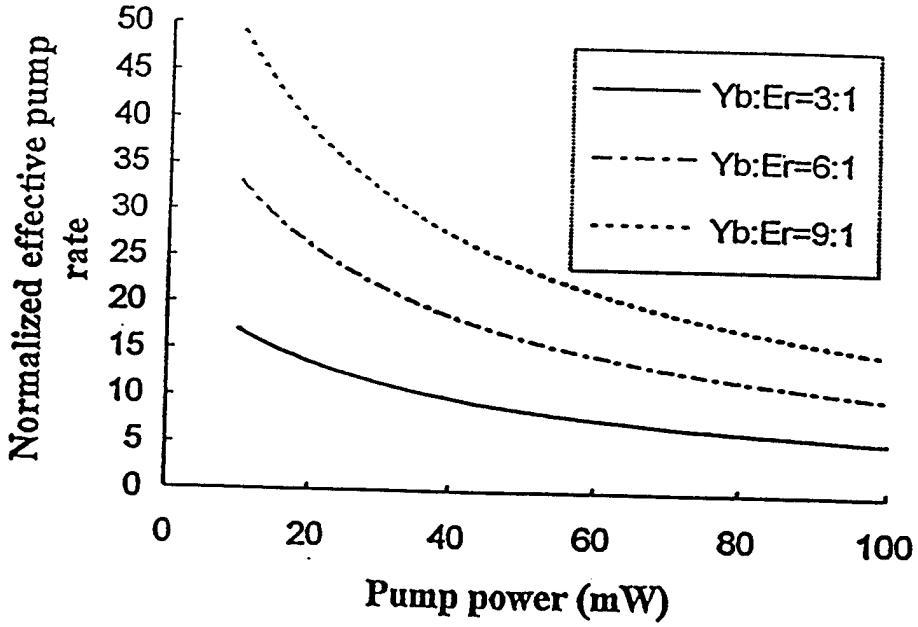

Fig. 8 Effective pump rate for various Yb:Er doping concentration ratios.

The laser dynamic behavior can now be described by coupled rate equations with a slight modification of (3) (4) and (5) by replacing R_p by $R_p^{Er} + \rho M_2$ to include the effect of Yb ions. For the steady state laser operation, the calculated effective pump rates for different Yb codoping concentration at λ pump=980nm are shown in Fig. 8. Results show that the enhancement of the pump rate by Yb ions becomes more effective when the pump power is relatively low. This fact is important for suppressing the ion-pair induced self-pulsing in Er-doped fiber lasers because the self-pulsing usually occurs at low to medium pump power level.

From a set of steady-state solutions, we obtain the stability conditions by solving the eigen-values of a new [A] matrix using the nominal values for all the parameters of Yb:Er codoped fibers and taking $\gamma = 1$ (the worst case). Fig. 9 shows the calculated stability diagrams on the x-Pp plane for different Yb:Er codoping concentrations, while keeping the same Er doping concentration. We see that for Yb:Er = 9: 1, the pump power required to suppress the self-pulsing for an ion-pair fraction of 30% is about 3mW, which is only 1/50 of the required power for the same ion-pair fraction without Yb codoping.

In summary, we have investigated the laser noises and instabilities in Er-doped and Yb:Er codoped fiber lasers. We showed that a small fluctuation in the pump laser power can lead to very large fluctuation in output laser power at relaxation oscillation frequency. Our results indicated that this instability can be suppressed by using high gain Er-doped fibers. However, with high-gain fibers, Q-switching or ion-pair induced self pulsing occurs, especially at low and medium laser pump power levels. This instability can be reduced by shifting the operating laser wavelength from the peak of the absorption at λ =1.535 um to high wavelengths. An alternative approach is to codope the fiber with Yb ions at very high concentration level to suppress the ion-pair-induced self-pulsing. By doing so it is possible to use high-gain or highly concentrated Er doped fibers for lasing media. Because of the very efficient energy transfer process that exists between Yb and Er, the introduction of Yb can significantly increase the pumping rate. As a result, ion-pair induced self pulsing in Er-fiber can be suppressed at relatively low diode laser pump power level. From the results of these analyses, we can establish useful scaling models for stable operation of cw fiber lasers.

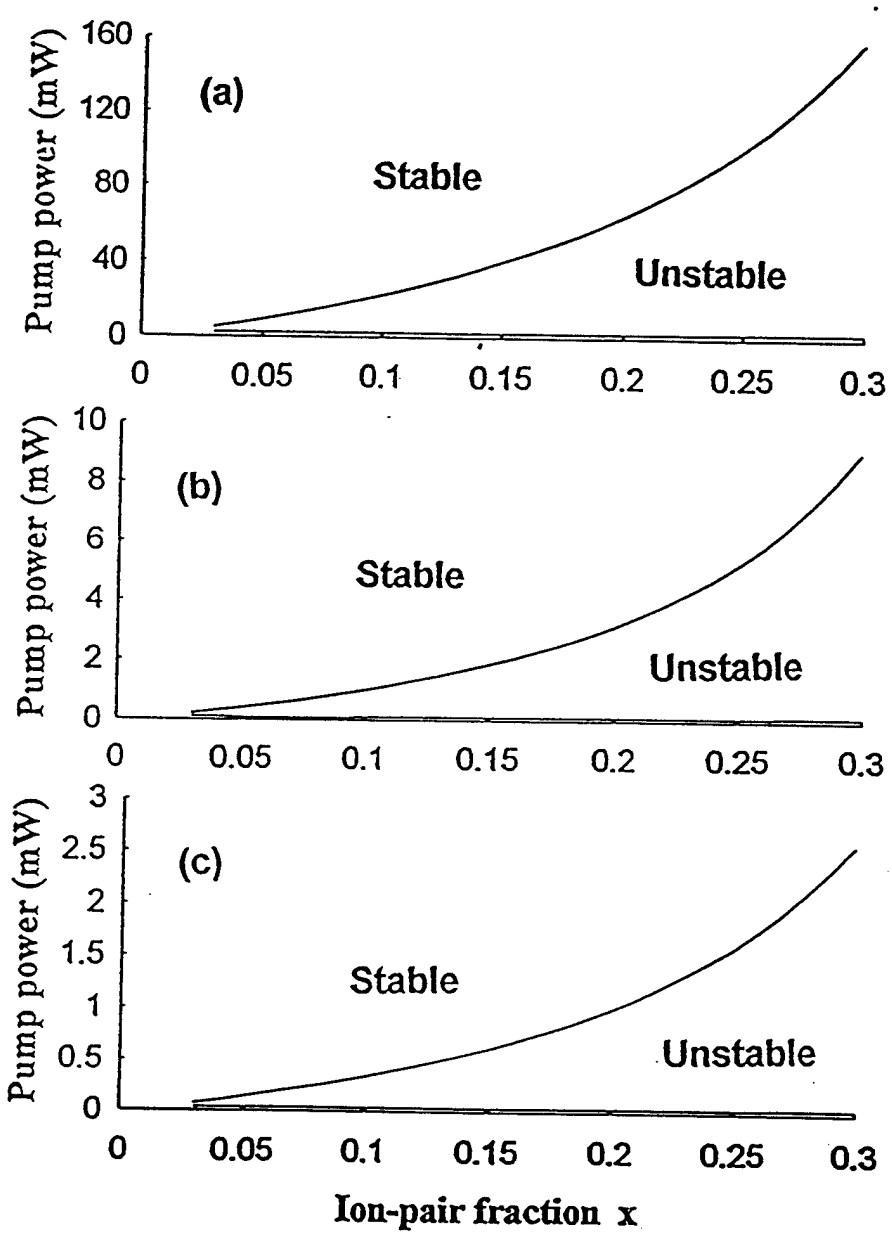

Fig. 9 Stability diagram for various Yb:Er doping concentration rations = (a) Yb:Er = 0 (b) Yb:Er = 3:1 and (c) Yb:Er = 9:1

5.0 All Optical Switch

5.1 CdSSe-Doped Fiber Fabrication And Characterization.

The fiber we fabricated had a core made of an RG630 Schott Glass material. The RG630 is a CdSSe/glass composite material in which the $CdS_{0.5}Se_{0.5}$ semiconductor is in the form of nano-spherical particles with average diameter of 3.7 nm and occupy a volume fraction of 0.32 percent. We had previously made theoretically modeling to indicate that, such a semiconductor doped fiber can have nonlinear refractive index higher than ordinary silica fiber and yet have losses low enough to be of practical significance.

The fiber cladding was fabricated from a B270 glass. A thick cladding wall was formed from two rods of B270 glass. The rods were drilled at the center to form glass tubes of inner and outer diameters of 0.212 inches and 1.35 inches respectively. The inner and outer diameters were polished to ensure a better surface for sealing during the draw process. One tube was drawn to 0.200 - 0.210 inches outer diameter by 0.03 inches inner diameter to fit inside the larger tube to build up the desired cladding wall thickness.

A core bar was produced by grinding and polishing a block of RG630 into a cylinder about 0.25 inches diameter by 6 inches long. It was then drawn to 0.029 inches outer diameter to fit the inner diameter of the inner tube in assembly. The assembly consisted of the three items described above assembled together. The core bar (0.29-inch diameter) was inserted into the smaller tube (0.02-in OD by 0.03-in ID). The smaller tube containing the core was then inserted into the larger tube (1.35-in OD x).212-in ID). The assembly was held together by mechanical means at the top end and attached to the feed mechanism of a draw tower. After the bottom of the assembly was heated and sealed, a vacuum was created inside the tubes allowing air pressure to collapse the tubes around the core, eliminating the air spaces between them during the drawing process.

The linear properties of the fiber was characterized in terms of its absorption coefficient and transmitivity. The experimental procedure for the absorption coefficient and for the transmittivity were based on the "Cut-back method" and the "White light source technique" respectively.

The transmittance of the fiber over a wavelength range between 380 and 1800 nm was measured using a tungsten filament white light source. The white light source was focused onto one end of approximately 16 cm length of the fiber. The output end of the sample fiber was focused onto the input aperture on an ANDO AQ1425 Optical Spectrum Analyzer. The transmission measurement of the Sample is shown in Figure 10. For comparison, the transmission measurement result of a 2.5 cm long rod of the RG630 core material is also included. The quantitative levels of the two measurements are greatly different. This difference is due to the diffraction limited focusing of the white light filament reducing the available power that can be launched into the core. qualitatively however, the position of a measured absorption edge is the same for both materials and

located near the expected value of 630 nm for this glass type. This results indicates that the CdSSe of the RG630 glass material survived the fiber fabrication process and should result in similar properties as that found in the bulk material.

A cut-back method was used to measure the linear absorption coefficient of the fiber. The source was a 1532 nm DFB pig-tailed semiconductor laser diode. The test fiber was mounted on two flexure stages. The pig-tailed laser was butt-coupled to one end of the fiber. An optical imaging system, located at the opposite end of the test fiber and comprised of an IR photocathode camera and a monitor, was used to observe and ensure that the source signal was well coupled into the core of the fiber before performing the cut-back measurement. Imaging results indicated that a large amount of scattering occurs in the sample fibers and is probably the largest contribution to the measured absorption coefficients. A standard single-mode fiber SMF-28 was used to collect the light from the sample fiber and deliver the power propagating in the core of the fiber to a photodiode detector. A Newport 835 power meter with an 818-IR detector was used to measure the output power.

An initial length (about 50 cm) of the test fiber was used. The output power was measured for different input power levels to ensure linear absorption. A known length of fiber was then cut-off from the detector end of the test fiber, and the output power again measured for the same set of input power levels. This procedure was repeated for additional cut-backs and an average of the results was made after calculating the absorption coefficient according to,

$$\alpha(dB/cm) = \frac{1}{L(cm)} 10 \log \frac{P_{out1}}{P_{out2}} \qquad (10)$$

where P_{out1} is the measured output power prior to cutting and P_{out2} is the measured output power after cut-back. The absorption coefficient was measured to be 0.14 dB/cm.

5.2 Measurement Of The Nonlinear Refractive Index

The experimental procedure for measurement of the nonlinear refractive index follows the Z-Scan technique. The measurement was made at 1313 nm using a 1313 nm Quantronics ND:YLF pulsed laser, with a pulse repetition rate of 100 MHz and a pulse width of 70 pS. The maximum average power of the laser is 1.4 W. The power was controlled with the variable attenuator. A microscope slide was used to split of a fraction of the laser beam, the beam was detected and served as the reference signal for the Z-SCAN measurements. The remaining portion of the laser was directed through a series arrangement of an isolator, mirror and a plano-convex mirror unto an RG630 sample. The sample was mounted on a translation stage. A detector, with a 100 μm aperture attached to it, was place 20 cm from the focal plane of the lens. The sample was scanned through the focal plane of the lens at intervals of 1 mm. The power of the two detectors were recorded at each new sample position, z. Normalized transmittance measured at power levels of 1.1

W, 1.2 W and 1.4 W. The transmittance was normalized to the transmittance at distances far away from the focal plane. From these measurements the nonlinear refractive index n_2 was determined using the equation.

$$n_2(esu) = \frac{\Delta T_{p-v}}{I_o(t)}\left[\frac{1}{0.046(1-S)^{0.25}}\right]\frac{2\pi}{\lambda}\frac{\alpha}{1-e^{-\alpha L}}\frac{2n_o}{40\pi} \qquad (11)$$

Here:

$\Delta T_{p-v} \equiv$ Peak-to-valley change in transmittance.

$I_O(t)$ - is the peak intensity of the laser source signal

S - is the aperture linear transmittance

L - Sample thickness

n_O - linear refractive index of fiber.

The nonlinear refractive index was calculated for the three power levels of 1.0W, 1.1 W, and 1.2W and an average was found to be $n_2 = 1.8 \times 10^{-17}$ m^2/W at 1313 nm.

First we performed an experiment to measure the induced wavelength shift of a 1550 nm probe by a 1319 nm pump. A CdSSe-doped fiber served as a Kerr nonlinear medium for the pump-probe interaction. Results of this experiment was valuable in determining the criteria needed to design and implement the optical switch. The experimental set up is as shown in figure 10.

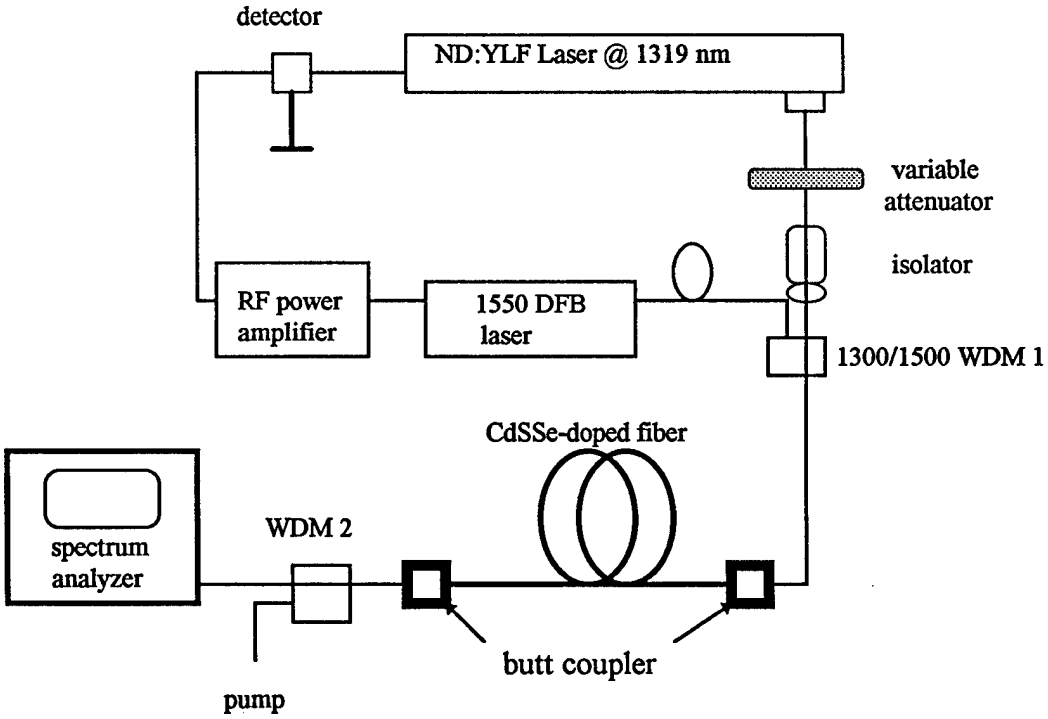

Fig. 10 Setup for measurement of 1319 nm pump-induced wavelength shift of a 1550 nm probe.

The pump was a Quantronix ND:YLF pulsed laser with emission wavelength of 1319 nm. The output pulses of the laser varied between 70 to 90 ps, with a pulse repetition rate of 100 Mhz. A variable attenuator was used to control the amount of pump power coupled into the fiber. An isolator was also introduced in the path of the pump to safe guard the laser against back reflections. The probe signal was a cw 1550 nm distributed-feedback (DFB) laser. The laser was gain switched to produce 70-90 ps pulses with a repetition rate of 100 Mhz. To gain switch the DFB laser, a fraction of the pump signal was tapped-off and directed unto a 20 Ghz detector. The detected signal was amplifier, by the RF power amplifier, and the amplified signal used to gain switch the DFB laser.

The pump and probe pulses were coupled into the CdSSe-doped fiber via a 2x1 1330/1550 nm wavelength division multiplier (WDM 1). The output of the WDM 1 was butt-coupled to one end of the CdSSe-doped fiber. The length of fiber used was 100 cm. Another 1330/1550 nm wavelength-division demultiplexer, WDM 2, was butt-coupled to the other end of the fiber. Finally, the output of the WDM 2 was connected to the spectrum analyzer.

A pump induced wavelength shift of 0.3 nm was measured. This was lower than the theoretically calculated wavelength shift of 1 nm according to the following formula:

$$\Delta\lambda_{probe} = -\frac{2\lambda_{probe}^2 n_2}{c\lambda_{pump}A_{eff}} P_p \frac{L_W}{T_o}$$

Here, λ_{probe}, and λ_{pump}, are the probe and pump wavelengths respectively. The non-linear refractive index of the CdSSe-doped fiber is n_2, P_p- is the peak pump power, L_w- is the walk-off length between the pump and probe, T_o- is the pulse-width which was taken as 2 ps, A_{eff}- is the effective area of the fiber, and c is the speed of light.

The failure to measure an appreciable pump induced wavelength shift of the probe was attributed to:

1) Wide pulse-width of pump and probe.
The pulse-width of the pump and the probe pulses used in the theoretical calculation was 2 ps. but the pulse-width of the pump and probe were between 70-90 ps. We attempted to compress the 70 ps pulses down to 2 ps, but was unsuccessful.

2) Pump absorption by the CdSSe-doped fiber.
Because of the relatively high loss of the CdSSe-doped fiber, 0.14 dB/cm, pump absorption in the 100 cm long fiber was significant. This meant that the pump-induced phase shift of the probe signal would be significantly lower. Since the wavelength shift is defined to be the time derivative of the

phase shift, the low phase shift translated into a small wavelength shift for the probe.

3) Jitter of Pump Signal.
The pump pulses were found to fluctuate or jitter. This caused a large walk-off between the pump and probe thereby reducing the interaction time of the pump and probe signals in the CdSSe-doped fiber.

We did not obtain pump and probe lasers that would provide short pulses (< 2 pS) as a results a practical whose operation was based on induced wavelength shift in a nonlinear CdSSe-Doped fiber could not be demonstrated.

Discussion/Conclusion.

We have successfully fabricated a CdSSe-doped fiber. Both its linear and nonlinear characteristics have been characterized. The transmittance of the fiber is constant for the wavelength range from 800 nm to 1800 nm. The Absorption coefficient was measured to be .14 dB/cm. This is about 10 times the theoretical limit for such semiconductor/glass composite. We believe that most of the loss occur at the core/cladding interface as we observed high scattering of the laser beam using a CCD camera. The nonlinear refractive index was measured to be $n_2 = 1.8 \times 10^{-17}$ m^2/W at 1313 nm. This value is 400 times higher than ordinary silica fiber. Therefore even with the relatively high loss, this fiber has the potential for implementing compact optical devices that can be actuated at laser diode power levels. We did not have very short (< 2 ps) pump and probe pulses in order to implement a practical fiber switch.

6. References

1. I.N. Duling III, Electr. Lett., 27 544 (1991)
2. V.J. Matsas, et.al., Electr. Lett., 28 1391 (1992)
3. O.G. Okhotinkov, et.al., IEEE Photo. Tech. Lett., 6 93 (1994)
4. F.M. Mitschke and L.F. Mollenaur, IEEE J. Quant. Elect. 22 2242 (1986)
5. E.P. Ippen, et.al., J. Opt. Soc. Am., B6, 1736 (1989)
6. U. Keller, et.al., "Ultrafast Phenomena VII", Belrin, Springer-Verlag (1990)
7. D.W. Huang, et.al., OSA CLEO Tech. Digest 11, (1997), CTHH4, P345.
8. M. Ding and P.K. Cheo, IEEE Photon. Tech. Lett., 8, 1151 (1996).
9. F. Sanchez, et. al., Phys. Rev. A, 48 2220 (1993)
10. P. LeBoudec, et. al., Opt. Quant. Electron., 25, 501 (1993)
11. M. Ding and P.K. Cheo, IEEE Photon. Tech. Lett., 8, 1627 (1996).